Letter

Network approach for the analysis of the irreversible deformation of solids with soft heterogeneities

Tito Andriollo [1,*] Varvara Kouznetsova,[2] and Laura Alessandretti [3]
[1]*Aarhus University, 8000 Aarhus C, Denmark*
[2]*Eindhoven University of Technology, 5600 MB Eindhoven, The Netherlands*
[3]*Technical University of Denmark, 2800 Kgs. Lyngby, Denmark*

(Received 28 January 2022; revised 15 June 2022; accepted 15 November 2022; published 29 November 2022)

We introduce the concept of shear band network (SBN) in ductile solids containing soft particles to investigate their irreversible deformation. Drawing on network science tools, we show that the evolution of the SBN explains the material strength at the coarse scale. To gain physical understanding of the activation order of the SBN links during tensile loading, we develop an analytical model based on the continuum theory of irreversible deformation. The results are used to construct an efficient, parameter-free indicator of the material strength that is solely based on the particle size and spatial distribution, thus proving that network science can advance the understanding of strength mechanisms in ductile solids.

DOI: 10.1103/PhysRevMaterials.6.L110601

Most solid materials are heterogeneous at scales larger than the atomic, yet considerably smaller than the size of the objects or components the materials are used for. The heterogeneity can stem from the subdivision into well-defined domains, e.g., crystals in polycrystalline metals, as well as from the presence of secondary phase particles and porosities [1]. This second type of heterogeneity is very common, and it is often of high concern due to its dramatic impact on the material behavior at the coarse scale. The effect can be either beneficial and purposely pursued, like in particle-reinforced composites and porous orthopedic implants [2,3], or heavily detrimental and cause for unpredicted failures, like undesired porosity in 3D printed metal parts [4]. Consequently, the development of reliable and efficient scale-bridging tools to predict the impact of such heterogeneity on the mechanical strength is imperative.

In ductile materials, the mechanical strength is defined by the stress σ_S at which irreversible deformation is observed at the coarse scale. The effect of particles and porosities—henceforth simply called particles—on σ_S can be estimated by assuming the material to be a continuum and applying methods based on continuum mechanics. Analytical approaches are fast but with limited applicability, as they use highly simplified assumptions about the particle size, shape, and spatial distributions [5–7]. Direct numerical simulation techniques do not suffer from this limitation, as they are based on numerical models of the whole material microstructure [8]. However, the maximum number of particles that can be included in a finite-element model is now a few hundred [9], which is still much smaller than the number of micrometer-sized particles forming the microstructure of real parts. A workaround is to limit the analysis to a representative element (RE) of the microstructure and to estimate the σ_S via computational homogenization techniques [10,11]. However, as the RE must be sufficiently large to be statistically representative, this approach can still be computationally very expensive [12].

The absence of a technique that is both *accurate enough* to account for microstructural heterogeneity and *efficient enough* to enable predictions based on a large number of particles has two adverse consequences. First, it precludes a synergistic coupling with modern, data-intensive characterization tools, e.g., x-ray tomography, which can provide accurate quantifications of the distribution of micrometer-sized particles in solids [13,14]. Second, it delays the development of new functionally graded materials with tailored particle distribution throughout the microstructure [15–19], as it prevents understanding the mechanisms governing the σ_S in the presence of many unevenly distributed particles.

In this Letter, we propose an approach to understand and predict the irreversible deformation that controls the strength of ductile materials containing soft particles. The key idea is to model the material as a network rather than as a continuum. Experimental and theoretical studies show that, in the presence of micrometer-sized soft particles, the irreversible deformation localizes in so-called shear bands (SBs) connecting the particles [20–23] (see Supplemental Fig. 1 in the Supplemental Material [24] and the associated references [9,25]). This suggests that the irreversible deformation can be modeled as a time-evolving network where the nodes represent the particles and the links represent the SBs. Network approaches have been successfully applied to investigate the deformation of granular materials [26–28]. In the following, we demonstrate that their application realm can also be extended to heterogeneous solids.

Consider a solid whose microstructure consists of particles embedded in a homogeneous isotropic matrix. The particles

*titoan@mpe.au.dk

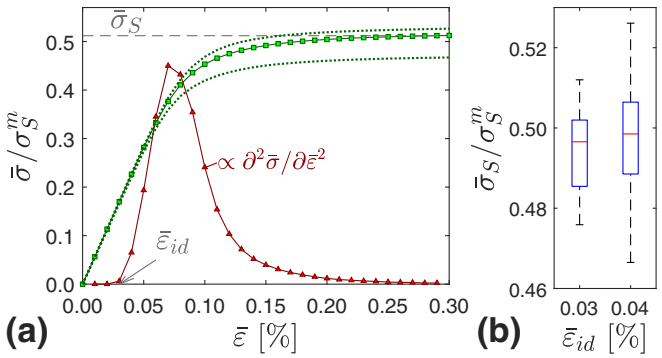

FIG. 1. (a) Mechanical response of the RE model (green solid line); $\bar{\sigma}$ is normalized by the matrix strength σ_S^m. Dotted lines indicate the min-max range across the RE set. The red line indicates the second derivative. (b) Statistical box plots showing the $\bar{\varepsilon}_{id}$ vs $\bar{\sigma}_S$ data for all REs (red line: median; box: interquartile range; whiskers: 2.5 and 97.5% percentiles). $\bar{\varepsilon}_{id}$ only takes discrete values due to the incremental solution strategy; see the Supplemental Material [24].

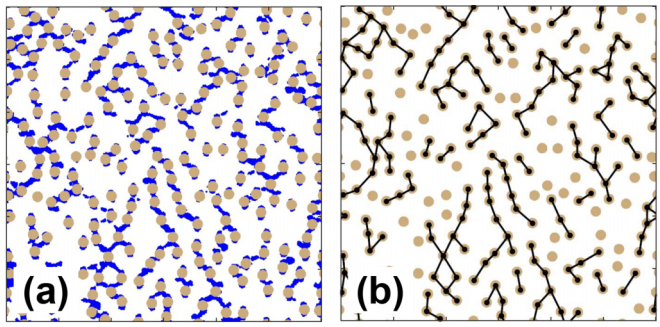

FIG. 2. (a) Example of irreversible deformation pattern in the matrix at $\bar{\varepsilon} = 0.1\%$ tensile strain in the horizontal direction, resulting from an RE simulation. Brown: particles; Blue: matrix undergoing irreversible deformation ($\dot{w}_i > 0$); White: matrix undergoing reversible deformation only ($\dot{w}_i = 0$). (b) SBN associated with the irreversible deformation pattern in (a).

are assumed "soft," i.e., with negligible stiffness compared to the matrix, e.g., voids. Following Ref. [29], we assume that such microstructure can be represented by a 2D square RE containing a uniform spatial distribution of circular holes generated via a random sequential absorption algorithm. The holes (particles) have radius R and the side length of the RE is $L = 60R$. The number of particles n_p is such that a particle area fraction of $f_p = 20\%$ is attained, which is often used as the reference for random heterogeneous media [30]. In total, 100 REs with different random realizations of the particle distribution are generated and subsequently subjected to uniaxial tension, simulated with the finite-element model described in the Supplemental Material [24,31], in which the matrix material is modeled as linear elastic-perfectly plastic [32] with strength σ_S^m. The effective deformation is measured by the scalar strain $\bar{\varepsilon} = \Delta L/L$, which corresponds to the relative elongation of the RE. The scalar effective stress needed to attain a certain value of $\bar{\varepsilon}$ is computed as $\bar{\sigma} = F/L$, where F is the overall reaction force on the RE.

The curve $\bar{\sigma}$ vs $\bar{\varepsilon}$ predicted by the model for one single RE is shown in Fig. 1(a). After an initial linear stage, the slope of the curve decreases gradually until the curve becomes almost flat. The reason is the irreversible deformation developing in the ductile matrix, which causes the nonlinear response. The point where the irreversible deformation is detectable in the effective response is identified by a nonzero zero value of the second-order derivative of the $\bar{\sigma}$ vs $\bar{\varepsilon}$ curve and it is marked with the symbol $\bar{\varepsilon}_{id}$. The effective stress at which the final plateau is reached corresponds to the material strength $\bar{\sigma}_S$, which we quantify following the 0.2% residual strain convention [1].

The spatial distribution of the particles has an impact on $\bar{\sigma}_S$ [33]. This effect is captured by the two dotted lines in Fig. 1(a), which represent the maximum and minimum values of the effective stress across the RE set. The variation in terms of $\bar{\sigma}_S$ is on the order of 10–15%. Although both $\bar{\varepsilon}_{id}$ and $\bar{\sigma}_S$ are influenced by the particle distribution, a statistical t test performed on the $\bar{\varepsilon}_{id}$ vs $\bar{\sigma}_S$ data—reported as boxplots in Fig. 1(b)—reveals that larger $\bar{\varepsilon}_{id}$ does not imply higher $\bar{\sigma}_S$ on average (p value $= 0.38$). This indicates that $\bar{\sigma}_S$ is mostly determined by the *progressive evolution* of the SBs inside the microstructure, rather than by the onset of the local irreversible deformation at the microscale.

To investigate the formation of SBs at strains larger than $\bar{\varepsilon}_{id}$, the output of the RE model in terms of the rate of local irreversible work per unit area $\dot{w}_i$ is used to define a time-dependent, unweighted, undirected spatial network [34] that represents the instantaneous pattern of irreversible deformation in the microstructure. This *shear band network* (SBN) is computed at discrete time points during the deformation process as follows. First, pairs of particles connected by SBs are identified from the scalar field $\dot{w}_i$ using the methodology described in the Supplemental Material [24], which, essentially, consists of subdividing the region where $\dot{w}_i > 0$ into domains of irreversible deformation, each associated with one particle. A SB exists between two particles if the corresponding domains are adjacent. Subsequently, the SBN is constructed by associating a *node* with each particle and a *link* with each pair of nodes for which the corresponding particles are connected by a SB. Figure 2 shows an example of the irreversible deformation pattern resulting from the RE simulation and the corresponding SBN.

An analysis of the evolution of the basic metrics of the SBN reveals its strong correlation with the macroscopic response of the material past $\bar{\varepsilon}_{id}$. Figure 3 compares the evolution of the number of connected components n_{cc}, i.e., the number of subnetworks in which any two nodes are reachable via a sequence of links [35], with the evolution of $\partial^2\bar{\sigma}/\partial\bar{\varepsilon}^2$, which can be interpreted as the rate at which the material stiffness varies (reduces) due to irreversible deformation. These two quantities are reported as average values across the RE set. In addition, the values of n_{cc} are normalized by n_p and $\partial^2\bar{\sigma}/\partial\bar{\varepsilon}^2$ is scaled to facilitate visual comparison. The figure clearly shows correlation between these two quantities. This fact is confirmed by the value of the Spearman rank coefficient ρ and its p value, which are 0.96 and 4.2×10^{-16}, respectively, as indicated in the figure. Remarkably, as demonstrated in Supplemental Fig. 4 [24], such correlation holds true also if the particle area fraction in the RE is 10% instead of 20%, if the particle spatial distribution is clustered instead of uniform,

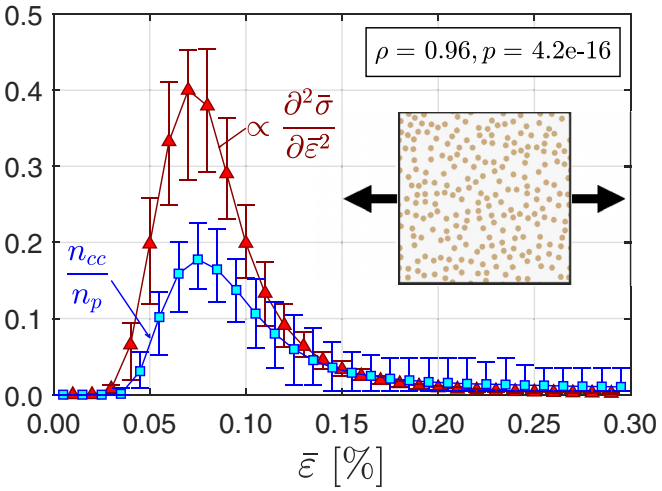

FIG. 3. Comparison between the evolution of the number of connected components n_{cc} (blue squares) and the evolution of $\partial^2\bar{\sigma}/\partial\bar{\varepsilon}^2$ (red triangles). The curves represent average values across the RE set, while the error bars indicate the corresponding max-min range.

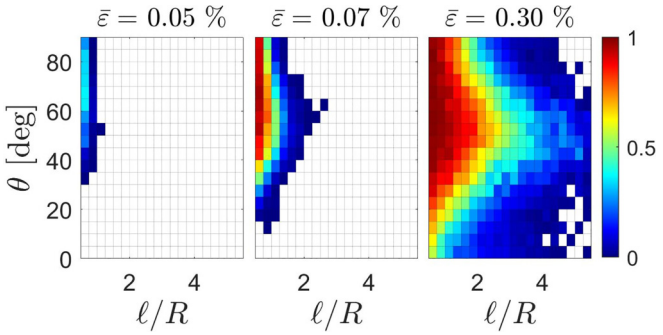

FIG. 4. Heatmaps showing the average fraction f_{AL} of Delaunay links with normalized length ℓ/R and orientation θ relative to the loading direction. Results are shown for several values of $\bar{\varepsilon}$. The value of f_{AL} corresponding to each color is shown in the colorbar; white corresponds to zero links.

or if the RE is subjected to other deformation modes, i.e., equibiaxial or shear, suggesting that the correlation has a general validity. Similar correlations can also be established with other SBN metrics; see Supplemental Fig. 5 [24].

Importantly, the findings from Fig. 3 hint that it is possible to estimate the material strength, $\bar{\sigma}_S$, based on properties of the SBN. The SBN, however, is not known *a priori*. Accordingly, we propose a method to identify a set of potential SBN links (the SBs) from the spatial distribution of particles alone, i.e., without performing computationally expensive RE simulations. Noticing that the SBN is planar, i.e., its links do not cross each other as discussed in the Supplemental Material [24], we compared the SBN with a prototypical planar network model, the Delaunay network defined by the particle centers [34]. The Delaunay network has a number of desirable properties including that all pairs of nearest-neighbor nodes are connected [36]. Considering the evolution of the SBNs for all simulations, we found that more than 95% of the SBN links exist in the corresponding Delaunay network (see Supplemental Fig. 6 [24]), regardless of the specific type of particle distribution, area fraction, and deformation mode. This implies that the SBN is essentially a subset of the Delaunay network. Consequently, we can henceforth consider the evolution of the former as a progressive activation of the links of the latter.

To investigate which links of the Delaunay network are active in the SBN, we examined the activation order of the Delaunay links by classifying them into bins based on their length ℓ, defined as the distance between the particle centers minus $2R$, and their orientation θ with respect to the direction of the tensile loading applied to the RE. For each bin and increment of $\bar{\varepsilon}$, the average fraction f_{AL} of active links was then computed across the RE set. The outcome is reported in Fig. 4. It can be noticed that the shortest links oriented at an angle between approximately 30° and 90° are the first to activate ($\bar{\varepsilon} = 0.05\%$). However, their fraction quickly saturates and longer links become active soon after ($\bar{\varepsilon} = 0.07\%$). This process continues until the distribution of f_{AL} stabilizes and reaches a nearly steady state at $\bar{\varepsilon} = 0.30\%$.

While the early activation of the shortest links is explained by higher local stresses in the matrix due to stress concentrations [5], the dependence of the link activation sequence on θ is not intutive. To justify it, we developed an analytical model, which considers the rate of irreversible work $\dot{W}_{SB}$ associated with a single SB. As detailed in the Supplemental Material [24], we assimilate the process of SB development in the REs to the mechanism of SB formation in a slab subjected to a biaxial stress state, where the ratio ξ between the principal stresses governs the SB orientation. By assuming that $\dot{W}_{SB}$ is done over an area proportional to ℓR, where ℓ indicates the SB length, we show that

$$\dot{W}_{SB} \propto \ell R \bar{\sigma} \dot{\bar{\varepsilon}} \left(1 + \xi(\theta) \frac{2\xi(\theta) - 1}{2 - \xi(\theta)} \right), \tag{1}$$

where $\dot{\bar{\varepsilon}}$ is the rate of macroscopic strain and the function $\xi(\theta)$ is implicitly defined by the equation

$$\cos(2\theta) = \frac{1 + \xi}{3(\xi - 1)}. \tag{2}$$

The estimate (1) holds at an early stage of irreversible deformation, when only few noninteracting SBs exist. Since the formation of SBs in solids can be regarded as a process where generalized rate of work is minimized [37], we expect the SBs requiring the least amount of mechanical work to form first. Accordingly, we assume the mean number of SBs of length ℓ and orientation θ at a given $\bar{\varepsilon}$ to be inversely proportional to $\dot{W}_{SB}(\ell, \theta)$. This leads, based on Eq. (1), to the following form of the function $f_{SB}(\ell, \theta)$ describing the distribution of the number of SBs per unit area:

$$f_{SB}(\ell, \theta) \propto \frac{R}{\ell} \chi(\theta), \tag{3}$$

with

$$\chi(\theta) = \begin{cases} \frac{2 - \xi(\theta)}{\xi(\theta)^2 - \xi(\theta) + 1} & \text{if } \theta > \theta^{cr} \\ 0 & \text{if } \theta \leqslant \theta^{cr} \end{cases}. \tag{4}$$

In Eq. (4) the condition on θ compared to $\theta^{cr} = (1/2)\cos^{-1}(1/3) \approx 35^\circ$ is introduced because the present

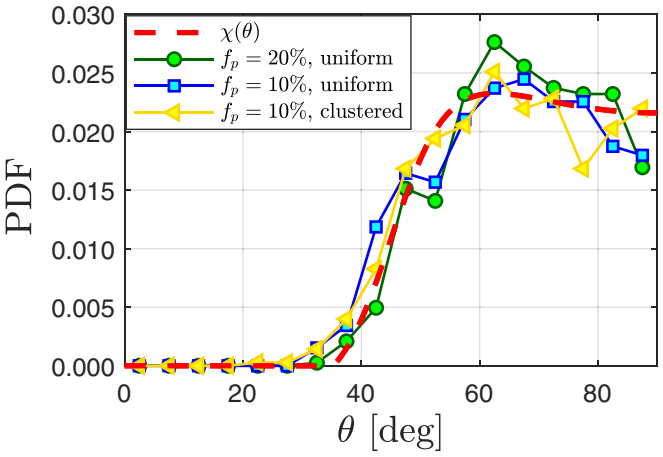

FIG. 5. Comparison between the function $\chi(\theta)$ (normalized to obtain unit area under the curve) and the angular distribution of the SBs obtained from SBN data at $\bar{\varepsilon} = 0.05\%$.

model rules out the possibility that SBs form at an angle $\theta \leqslant \theta^{cr}$ (see the Supplemental Material [24]). To verify Eq. (3), we used the SBN data to compute the mean angular distribution of the SBs of any length at $\bar{\varepsilon} = 0.05\%$. According to Eq. (3), such distribution is expected to be proportional to $\chi(\theta)$:

$$f_{SB}(\theta) = \int_{\ell_{\min}}^{\ell_{\max}} f_{SB}(\ell, \theta) d\ell \propto \chi(\theta). \tag{5}$$

Figure 5 demonstrates that this is indeed the case, regardless of the specific type of particle spatial distribution and particle area fraction within the investigated range.

Therefore, Eq. (3) and the fact that the SBN is a subset of the Delaunay network can be exploited to construct an inexpensive and parameter-free indicator of the material strength that is solely based on the particle size and spatial distribution. First, given a distribution of particles in a microstructure (e.g., from microscopy or x-ray tomography), the set of potential SBs are identified with the set of links of the Delaunay network. Next, the Delaunay links are classified into bins, based on their length ℓ and orientation θ. Finally, the *strength indicator* I_S is computed as follows:

$$I_S = \frac{1}{n_L^{\text{tot}}} \frac{\sum_{i,j} f_{SB}(\ell^i, \theta^j) n_L(i, j)}{\sum_{i,j} f_{SB}(\ell^i, \theta^j)}, \tag{6}$$

where ℓ^i and θ^j denote the mean values of ℓ and θ in the bin (i, j), $n_L(i, j)$ is the number of Delaunay links in the bin (i, j), n_L^{tot} is the total number of Delaunay links and $f_{SB}(\ell^i, \theta^j)$ is computed via Eqs. (3) and (4). For higher I_S, a lower material strength is expected, because large I_S means that the Delaunay network contains many links with low $\dot{W}_{SB}$, which activate early upon loading, thereby generating more irreversible deformation that reduces $\bar{\sigma}_S$. To support this argument, we computed I_S for all REs and analyzed its correlation with the values of $\bar{\sigma}_S$ predicted by the finite-element simulations. Table I lists the coefficient of determination R^2 and p value obtained from a linear regression of the $\bar{\sigma}_S$ vs I_S data, for different values of f_p and two types of particle spatial distribution. The p values are always below 1×10^{-4}, indicating a significant correlation between the two quantities.

TABLE I. Outcome of linear regressions between the material strength $\bar{\sigma}_S$ and our strength indicator I_S and between $\bar{\sigma}_S$ and the disorder parameter I_D.

f_p		$\bar{\sigma}_S$ vs I_S		$\bar{\sigma}_S$ vs I_D	
(%)	Particle distribution	R^2	p value	R^2	p value
20	Uniform	0.33	3.8×10^{-10}	0.17	1.5×10^{-5}
15	Uniform	0.29	1.4×10^{-8}	0.07	7.1×10^{-3}
10	Uniform	0.21	1.5×10^{-6}	0.11	7.2×10^{-4}
10	Clustered	0.15	9.5×10^{-5}	0.03	8.8×10^{-2}

However, the scatter is high (see the Supplemental Material [24]), leading to values of R^2 between 0.15 and 0.33. Yet, such values are 2–5 times larger than those associated with the correlation between $\bar{\sigma}_S$ and the state-of-the-art disorder parameter I_D used to estimate the strength of porous brittle materials [38]. This supports the earlier statement that if the matrix is ductile, the strength is not controlled by the onset of the irreversible deformation like in the brittle case, but rather by its evolution through the SBs.

Finally, we tested the ability of our strength indicator to capture the effect of the particle area fraction f_p, besides that of the particle spatial distribution. We found that within the considered range of f_p (see Fig. 6) the strength indicator I_S captures very well the inverse proportionality between $\bar{\sigma}_S$ and f_p. Indeed, if f_p increases, ℓ decreases and the irreversible deformation can propagate more easily because shorter SBs need to be formed. This feature of I_S looks appealing, because, in contrast to, e.g., the disorder parameter I_D or available analytical models focusing on the effect of f_p [6], it allows comparing the strength of materials where both the particle spatial distribution *and* f_p vary simultaneously.

In conclusion, this Letter demonstrates that network analysis approaches are powerful tools to understand and predict the irreversible deformation that controls the strength of heterogeneous solids containing particles and pores. The proposed concept of SBN is the key in this respect, as it provides

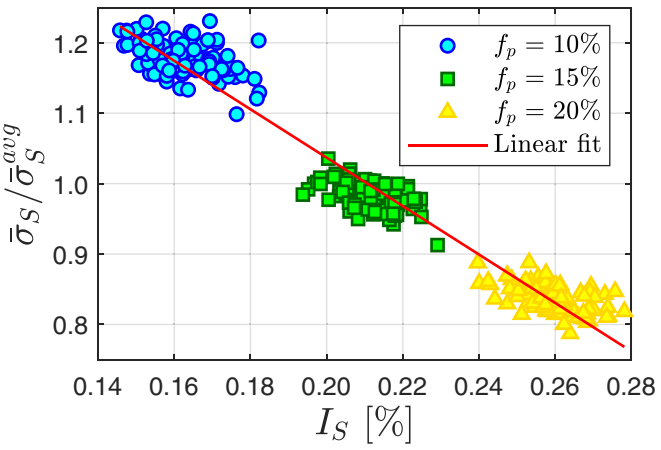

FIG. 6. Correlation between $\bar{\sigma}_S$ and I_S, considering data for three values of f_p and 100 realizations of the RE particle distribution for each f_p. The $\bar{\sigma}_S$ values are normalized by their mean, $\bar{\sigma}_S^{\text{avg}}$. The linear fit is meant to be a guide for the eyes only.

the connection between network and materials sciences. The present investigation can be extended along multiple directions, including a comprehensive study of the SBN properties for different deformation modes and of the effect of particles with stiffness greater than that of the matrix. Drawing on network science tools, our work opens an avenue towards developing models that account for the material heterogeneity while being more efficient and easier to evaluate than classical continuum mechanics and finite-element models.

T.A. thanks R. Aghababaei from Aarhus University for fruitful scientific discussions.

[1] M. Ashby, H. Shercliff, and D. Cebon, *Materials: Engineering, Science, Processing and Design* (Butterworth-Heinemann, Oxford, UK, 2010).

[2] N. E. Putra, M. J. Mirzaali, I. Apachitei, J. Zhou, and A. A. Zadpoor, Multi-material additive manufacturing technologies for Ti-, Mg-, and Fe-based biomaterials for bone substitution, Acta Biomater. **109**, 1 (2020).

[3] J. Aboudi, S. Arnold, and B. Bednarcyk, *Micromechanics of Composite Materials: A Generalized Multiscale Analysis Approach* (Butterworth-Heinemann, Oxford, UK, 2012).

[4] D. D. Ben, Y. R. Ma, H. J. Yang, L. X. Meng, X. H. Shao, H. Q. Liu, S. G. Wang, Q. Q. Duan, and Z. F. Zhang, Heterogeneous microstructure and voids dependence of tensile deformation in a selective laser melted AlSi10Mg alloy, Mater. Sci. Eng. A **798**, 140109 (2020).

[5] T. L. Anderson, *Fracture Mechanics – Fundamentals and Applications*, 3rd ed. (CRC Press, Boca Raton, 2005).

[6] G. Rousselier, Porous plasticity revisited: Macroscopic and multiscale modeling, Int. J. Plast. **136**, 102881 (2021).

[7] J. Faleskog and P. Gudmundson, Analytical predictions of yield stress of a strain gradient plasticity material reinforced by small elastic particles, J. Mech. Phys. Solids **157**, 104623 (2021).

[8] J. E. Bishop, J. M. Emery, C. C. Battaile, D. J. Littlewood, and A. J. Baines, Direct numerical simulations in solid mechanics for quantifying the macroscale effects of microstructure and material model-form error, JOM - J. Miner. Met. Mater. Soc. **68**, 1427 (2016).

[9] T. Andriollo, Y. Zhang, S. Fæster, J. Thorborg, and J. Hattel, Impact of micro-scale residual stress on in-situ tensile testing of ductile cast iron: Digital volume correlation vs. model with fully resolved microstructure vs. periodic unit cell, J. Mech. Phys. Solids **125**, 714 (2019).

[10] K. Matouš, M. G. D. Geers, V. G. Kouznetsova, and A. Gillman, A review of predictive nonlinear theories for multiscale modeling of heterogeneous materials, J. Comput. Phys. **330**, 192 (2017).

[11] J. Segurado, R. A. Lebensohn, and J. Llorca, Computational homogenization of polycrystals, in *Advances in Crystals and Elastic Metamaterials, Part 1*, edited by M. I. Hussein (Elsevier, Cambridge, MA, USA, 2018).

[12] S. Bargmann, B. Klusemann, J. Markmann, J. E. Schnabel, K. Schneider, C. Soyarslan, and J. Wilmers, Generation of 3D representative volume elements for heterogeneous materials: A review, Prog. Mater. Sci. **96**, 322 (2018).

[13] H. Villarraga-Gómez, E. L. Herazo, and S. T. Smith, X-ray computed tomography: From medical imaging to dimensional metrology, Precis. Eng. **60**, 544 (2019).

[14] T. M. Pollock, Alloy design for aircraft engines, Nat. Mater. **15**, 809 (2016).

[15] A. Sola, D. Bellucci, and V. Cannillo, Functionally graded materials for orthopedic applications – an update on design and manufacturing, Biotechnol. Adv. **34**, 504 (2016).

[16] P. S. Ghatage, V. R. Kar, and P. E. Sudhagar, On the numerical modelling and analysis of multi-directional functionally graded composite structures: A review, Compos. Struct. **236**, 111837 (2020).

[17] X. Wu and Y. Zhu, Heterogeneous materials: A new class of materials with unprecedented mechanical properties, Mater. Res. Lett. **5**, 527 (2017).

[18] E. Tejado, W–Cu metal matrix composites for next generation fusion devices, Mater. Today **38**, 136 (2020).

[19] S. Tarancón, E. Tejado, M. Richou, and J. Y. Pastor, Evaluation of tensile and elastic properties of W/Cu cold-spray coatings for application to the FGM DEMO divertor concept, Fusion Eng. Des. **171**, 112719 (2021).

[20] N. Bilger, F. Auslender, M. Bornert, J. C. Michel, H. Moulinec, P. Suquet, and A. Zaoui, Effect of a nonuniform distribution of voids on the plastic response of voided materials: A computational and statistical analysis, Int. J. Solids Struct. **42**, 517 (2005).

[21] F. Fritzen, S. Forest, T. Böhlke, D. Kondo, and T. Kanit, Computational homogenization of elasto-plastic porous metals, Int. J. Plast. **29**, 102 (2012).

[22] A. Buljac, L. Helfen, F. Hild, and T. F. Morgeneyer, Effect of void arrangement on ductile damage mechanisms in nodular graphite cast iron: In situ 3D measurements, Eng. Fract. Mech. **192**, 242 (2018).

[23] C. L. Xu, T. Andriollo, Y. B. Zhang, J. C. Hernando, J. Hattel, and N. Tiedje, Micromechanical impact of solidification regions in ductile iron revealed via a 3D strain partitioning analysis method, Scr. Mater. **178**, 463 (2020).

[24] See Supplemental Material at http://link.aps.org/supplemental/10.1103/PhysRevMaterials.6.L110601 for (1) example of shear band network in a real material, (2) description of the finite element model, (3) procedure used to identify the links of the shear band network, (4) shear band network metrics vs. material stiffness variation, (5) shear band network metrics vs. Delaunay network, (6) derivation of the rate of irreversible work for a shear band, and (7) strength indicator vs. material strength data.

[25] N. Limodin, J. Réthoré, J. Y. Buffière, A. Gravouil, F. Hild, and S. Roux, Crack closure and stress intensity factor measurements in nodular graphite cast iron using three-dimensional correlation of laboratory X-ray microtomography images, Acta Mater. **57**, 4090 (2009).

[26] L. Papadopoulos, J. G. Puckett, K. E. Daniels, and D. S. Bassett, Evolution of network architecture in a granular material under compression, Phys. Rev. E **94**, 032908 (2016).

[27] L. Papadopoulos, M. A. Porter, K. E. Daniels, and D. S. Bassett, Network analysis of particles and grains, J. Complex Networks **6**, 485 (2018).

[28] K. P. Krishnaraj and P. R. Nott, Coherent Force Chains in Disordered Granular Materials Emerge from a Percolation of Quasilinear Clusters, Phys. Rev. Lett. **124**, 198002 (2020).

[29] V. A. Buryachenko, R. Y. Kim, N. J. Pagano, and J. E. Spowart, Quantitative description and numerical simulation of random microstructures of composites and their effective elastic moduli, Int. J. Solids Struct. **40**, 47 (2003).

[30] C. L. Y. Yeong and S. Torquato, Reconstructing random media, Phys. Rev. E **57**, 495 (1998).

[31] V.-D. Nguyen, E. Béchet, C. Geuzaine, and L. Noels, Imposing periodic boundary condition on arbitrary meshes by polynomial interpolation, Comput. Mater. Sci. **55**, 390 (2012).

[32] E. de Souza Neto, D. Peric, and D. R. J. Owens, *Computational Methods for Plasticity: Theory and Applications* (Wiley, Chichester, UK, 2008).

[33] K. Sieradzki and R. Li, Fracture Behavior of a Solid with Random Porosity, Phys. Rev. Lett. **56**, 2509 (1986).

[34] M. Barthelemy, *Morphogenesis of Spatial Networks* (Springer International Publishing, Cham, Switzerland, 2018).

[35] M. Newman, *Networks: An Introduction* (Oxford University Press, Oxford, UK, 2010).

[36] Y. Malkov, A. Ponomarenko, A. Logvinov, and V. Krylov, Approximate nearest neighbor algorithm based on navigable small world graphs, Inf. Syst. **45**, 61 (2014).

[37] C. Miehe and M. Lambrecht, Analysis of microstructure development in shearbands by energy relaxation of incremental stress potentials: Large-strain theory for standard dissipative solids, Int. J. Numer. Methods Eng. **58**, 1 (2003).

[38] H. Laubie, F. Radjai, R. Pellenq, and F. J. Ulm, Stress Transmission and Failure in Disordered Porous Media, Phys. Rev. Lett. **119**, 075501 (2017).